RSC Advances

RSC Publishing

PAPER

View Article Online
View Journal | View Issue

Highly efficient organic light-emitting devices by introducing traps in the hole-injection layer

Cite this: *RSC Advances*, 2013, **3**, 14616

Wenyu Ji,[a] Jing Wang,[b] Qinghui Zeng,[a] Zisheng Su[a] and Zaicheng Sun*[a]

Received 10th May 2013,
Accepted 4th June 2013

DOI: 10.1039/c3ra42320d

www.rsc.org/advances

We introduced Pt_3Co nanoparticles (NPs) into the hole-injection layer (HIL) in organic light-emitting devices and demonstrated a highly efficient green OLED. The Pt_3Co NPs as the hole-traps adjusted the hole transport property in the PEDOT:PSS layer, consequently resulting in a balanced charge injection into the emission layer and enhancing the efficiency of the devices. The theory analysis also indicated that the hole traps induced by Pt_3Co NPs played an important role in improving the charge balance in the Pt_3Co-containing devices. The studies on the transient resolution photoluminescence (TRPL) indicated that the lifetime of the excitons was not influenced by the Pt_3Co NPs, even though a very thin spacer was introduced. The Pt_3Co-containing device exhibited a 73% higher current efficiency compared with the conventional device without Pt_3Co NPs.

1. Introduction

Organic light-emitting devices (OLEDs) have attracted much attention in the past tens of years due to their application in full color flat-panel displays (FPDs), automobiles, and lighting sources,[1,2] and one of the major advantages of OLED technology is the use of light weight flexible substrates and making flexible displays.[3–5] Many commercialization products and prototypes based on OLEDs have been unveiled because of the rapid progress in academia and industry research efforts on OLEDs.[6,7] This is shown by the large number of start-up companies and major corporations developing OLED based applications, such as Samsung, LG, Sony, Intel, Plastic Logic and so on. However, improving the performance of the OLEDs is still necessary for low cost and widely commercial applications of the OLEDs in displays and solid-state lighting. One major focus in OLED research is to improve the device luminance efficiency. According to the commonly accepted theory, the external quantum efficiency (η_{ext}) of an OLED is described by the equation[8,9]

$$\eta_{ext} = \gamma \times \varphi_{int} \times \eta_{ex} \times \eta_{out} \quad (1)$$

where γ is the electron–hole charge balance factor (the ratio of the number of electrons to the number of holes injected from opposite electrodes), φ_{int} is the intrinsic photoluminescence quantum yield for excitons (including both fluorescence and phosphorescence), η_{ex} is the fraction of excitons of specific multiplicity formed upon charge recombination ($\eta_{ex} \approx 1/4$ for singlet excitons and $\eta_{ex} \approx 3/4$ for triplet excitons), and η_{out} is the light out-coupling efficiency. In principle, the device efficiency can be improved through optimizing each parameter in this equation. Much effort has been devoted to designing new materials (including emitters and host materials) with higher photoluminescence quantum yields,[10,11] a novel device structure for maximizing light out-coupling,[12] and using different electrode/organic functional materials to improve the device efficiency.[13–15] A much less well focused parameter is the electron–hole charge balance factor, γ. At present, many reports have focused on modifying the metal–organic interface to reduce the interface barrier to charge injection. The interface barrier is originated from the different energy-level alignments of the metal work function and the highest occupied molecular orbital (HOMO) or the lowest unoccupied molecular orbital (LUMO) of the organic molecule according to the type of charges to be injected. In general, reducing the energy barrier between the electrode and organic functional layer is necessary for higher charge injection efficiency. However, with the suitable organic semiconductors and electrode materials available nowadays, it is very easy to adjust the energy alignment and either charge injection carrier (hole or electron) could become the minor carrier[16] *i.e.*, efficient charge injection and transfer are possible when metal oxides are introduced into OLEDs, such as $CsCo_3$, and transition metal oxides like molybdenum oxide (MoO_3), tungsten oxide (WO_3) and rhenium oxide (ReO_3).[17–22] Improving the injection of carriers that are already in excess can improve the absolute luminance due to the greater chance of charge recombination but can also have a deleterious effect on the efficiency because of the deteriorated balance in charge

[a]*State Key Laboratory of Luminescence and Applications, Changchun Institute of Optics, Fine Mechanics and Physics, Chinese Academy of Sciences (CAS), Changchun 130033, China. E-mail: jlu__jwy@163.com; sunzc@ciomp.ac.cn; Tel: +86-431-86176313*

[b]*School of Physics and Technology, University of Jinan, Jinan 250022, People's Republic of China*

carriers. Thus, the charge balance in a device is rather important in choosing the strategy needed to improve the device efficiency. For a given set of organic semiconductors in a device, the dopant of the hole–electron transport–injection layer greatly affects the charge transport from the electrode to the organic semiconductor, consequently influencing the charge balance in the device. The current density (J) crossing the device can be calculated by[23]

$$J = N_{\mathrm{HOMO}}\mu q^{1-m}\left(\frac{\varepsilon_0\varepsilon_r}{H_t}\right)^m \frac{V^{m+1}}{d^{2m+1}}C(m) \quad (2)$$

$$C(m) = m^m(2m+1)^{m+1}(m+1)^{-2m-1}[\sin(\pi/m)/g(\pi/m)]^m$$

Where N_{HOMO} is the HOMO effective density of states, μ is the carrier mobility, q is the electronic charge, $\varepsilon_0\varepsilon_r$ is the dielectric permittivity, H_t is the total trap density, V is the bias voltage, d is the thickness of the device and g is the trap degeneracy. For organic semiconductors using OLEDs nowadays, the mobility of hole in hole transport–injection materials is higher than that of electron in electron transport materials, which means that the hole will be in excess over electrons in the devices and leads to a charge imbalance. According to eqn (2), we can introduce hole traps, *i.e.*, by increasing the value of H_t in the hole injection layer (HIL) or/and the hole transport layer (HTL) to reduce the hole injection and transport in the device and improve the charge balance.

In this work, we demonstrated successful fabrication of efficient green OLEDs with PEDOT:PSS doped by Pt_3Co nanoparticles (NPs) as the HIL. An enhancement of about 73% is achieved for the peak efficiency and the maximum current efficiency of 76.4 cd A^{-1} was obtained under the luminance of 173 cd m^{-2}. The efficiency of 72.0 cd A^{-1} was obtained under the luminance of 1000 cd m^{-2}.

2. Experimental

The OLEDs consisted of glass/ITO/PEDOT:PSS:Pt_3Co (20 nm)/CBP (x nm)/CBP:Ir(ppy)$_3$ (12 vol.%, 45 nm)/TPBi (35 nm)/LiF (1 nm)/Al (200 nm). x is 0, 5, 10, and 15 nm for device A, B, C, and D, respectively. CBP is 4,4-*N*,*N*-dicarbazole-biphenyl, Ir(ppy)$_3$ is *fac*-tris(2-phenylpyridine) iridium, and TPBi is 1,3,5-tri(1-phenyl-1*H*-benzo[d]imidazol-2-yl)phenyl. The ITO glass substrates were cleaned in an ultrasonic bath with isopropyl alcohol, acetone, and methanol sequentially. PEDOT:PSS (Baytron PH):Pt_3Co was spin-cast from aqueous solution at 3500 rpm for 60 s to form a film of 20 nm thickness. The concentration of the Pt_3Co nanoparticles in PEDOT:PSS was 0.1 wt.%. The PEDOT:PSS:Pt_3Co film was annealed at 110 °C for 30 min in a glove box (MBRAUN) to obtain a highly conductive layer. Then, an organic hole-transport material, CBP, with emission layer CBP:Ir(ppy)$_3$, LiF, and Al were successively deposited by thermal evaporation at a pressure below 4×10^{-6} Torr. The layer thickness and the deposition rate of the materials were monitored *in situ* using an oscillating quartz thickness monitor. The deposition rates of organic materials, LiF, and Al were controlled to 0.2, 0.05, and 0.5 nm s^{-1}, respectively. In order to compare, the control device (device E) with a similar structure to device B using PEDOT:PSS instead of PEDOT:PSS:Pt_3Co, was fabricated. The characteristics of current–voltage and luminance were measured by a programmable Keithley model 2400 power supply and a Minolta Luminance Meter LS-110, respectively, in air at room temperature. The spectra of the devices were measured with an Ocean Optics Maya 2000-Pro spectrometer. For all devices, no external package or encapsulation was applied after device fabrication. Time-resolved photoluminescence (TRPL) measurements were carried out with an Edinburgh Instruments FL920 Spectrometer. For the TRPL measurements, the samples were fabricated on a quartz glass substrate and all the films were fabricated using the same technique described above. Various samples for TRPL measurements are as follows:

S-a: Substrate/PEDOT:PSS:Pt_3Co (20 nm)/CBP:Ir(ppy)$_3$ (12 vol.%, 10 nm); S-b: Substrate/PEDOT:PSS:Pt_3Co (20 nm)/CBP (5 nm)/CBP:Ir(ppy)$_3$ (12 vol.%, 10 nm); S-c: Substrate/PEDOT:PSS:Pt_3Co (20 nm)/CBP (10 nm)/CBP:Ir(ppy)$_3$ (12 vol.%, 10 nm); S-d: Substrate/PEDOT:PSS:Pt_3Co (20 nm)/CBP (15 nm)/CBP:Ir(ppy)$_3$ (12 vol.%, 10 nm); S-e: Substrate/PEDOT:PSS (20 nm)/CBP:Ir(ppy)$_3$ (12 vol.%, 10 nm).

3. Results and discussion

Monodisperse Pt_3Co NPs are synthesized through an organic solvothermal approach modified from previous publications.[24] Co-based alloy NPs and nanowires have been employed in OLEDs, such as CoFe NPs[25] and $Pt_{47}Co_{53}$ nanowires.[26] However, Pt_3Co NPs, which are often used as the catalyst for the oxygen reduction reaction,[27] have not been reported to have been used in OLEDs to date. Here we focus on the effect of Pt_3Co NPs on the hole injection–transport in the PEDOT:PSS layer. Fig. 1 shows the SEM images of PEDOT:PSS and PEDOT:PSS:Pt_3Co on ITO substrates. A homogeneous layer is obtained by pure PEDOT:PSS spin-coating the substrate. Different contrast regions in Fig. 1b can be seen, with the bright white one assigned to the Pt_3Co NPs. Inset is the TEM image of Pt_3Co NPs that are spherical with a diameter of ~7 nm. The Pt_3Co NPs are randomly distributed in the PEDOT:PSS layer and are nearly monodisperse. Fig. 2a shows the schematic structures with and without Pt_3Co NPs in the PEDOT:PSS layer. The PEDOT:PSS (PEDOT:PSS:Pt_3Co) layer is used as the HIL, neat CBP as the HTL and spacer, CBP:Ir(ppy)$_3$ as the emitting layer, TPBi as the electron transport layer (ETL) and LiF/Al as the cathode. Fig. 2b shows the voltage–current density characteristics of all the devices. The J–V characteristics of these devices are well described by the power law of $J \propto V^{m+1}$. The devices with Pt_3Co NPs exhibit similar J–V characteristics due to the same HIL in these devices. The value of m is ~8.7 and ~11.7 for devices without Pt_3Co and with

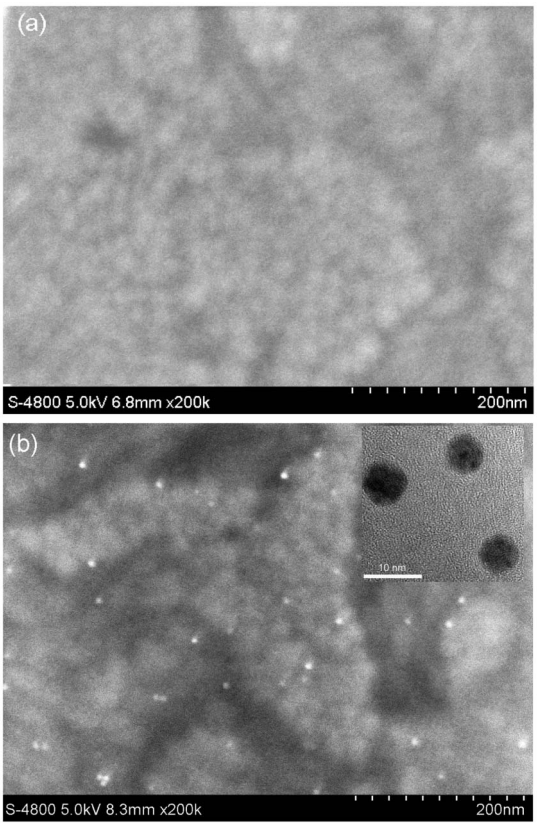

Fig. 1 The SEM images of (a) PEDOT: PSS and (b) PEDOT:PSS:Pt_3Co on ITO substrates. Inset is the TEM image of Pt_3Co NPs.

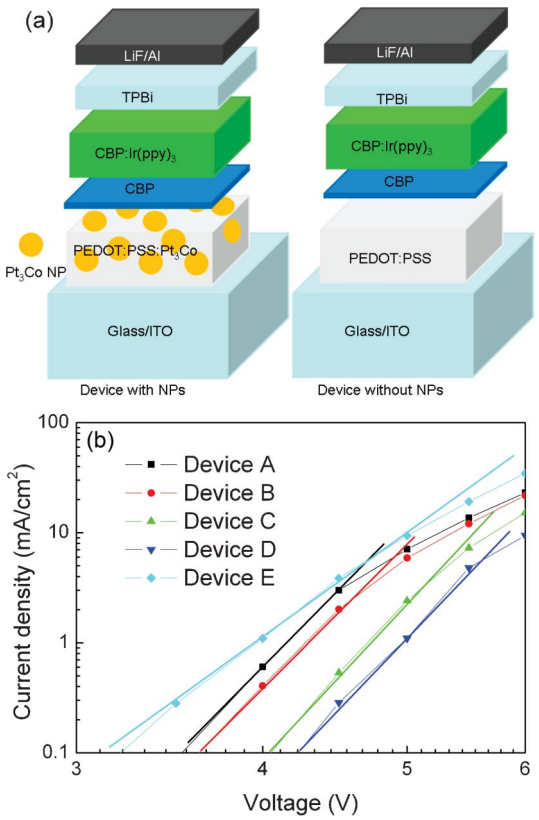

Fig. 2 (a) The schematic device structures with and without Pt_3Co NPs; (b) the current density–voltage characteristics of devices A, B, C, D, and E.

Pt_3Co NPs. The value of m increases with the introduction of Pt_3Co NPs, suggesting that Pt_3Co NPs serve as hole traps and lead to an increased turn-on voltage. The current density of devices with Pt_3Co NPs decreases with increasing the thickness of CBP, which is due to the increase of the device thickness. We can see that the value of m is similar even though the CBP thickness increases, which also demonstrates that the larger m in the Pt_3Co NP containing device is originated from the increased hole-trap density induced by Pt_3Co NPs in PEDOT:PSS. A similar phenomenon has been reported by Sun *et al.*[25]

Fig. 3a shows the current density–efficiency characteristics of all the devices. We can see that the efficiency of device A is lower than that of device E, which is ascribed to the quenching effect of Pt_3Co NPs on excitons, as disscussed in the next paragraph. The device efficiency is improved with the introduction of a CBP spacer, which separates the Pt_3Co NPs from the emission layer and avoids exciton quenching. It can also be found that the device efficiency is further improved with the spacer thickness increasing. We explain this phenomenon as follows. A thicker spacer will increase the time of holes injecting into the emission layer from the ITO anode, which should further balance the charge in the emission layer. In addition, we have fabricated the control device with the same architecture as device D, named device F, and a little enhancement for device F relative to device E, which is not consistent with devices B and D. This can be due to the thicker CBP spacer decreasing the leakage resulting from the aggregation of Pt_3Co NPs in PEDOT:PSS in a Pt_3Co NP based device, as can be seen in Fig. 1b. We can conclude that the performance enhancement of device D relative to device A is due to the three reasons, (1) the decrease of exciton quenching by Pt_3Co NPs, (2) a more balanced charge injection and (3) the decrease of leakage current.

In principle, we can also decrease the thickness of the ETL to reduce the time of electron injection into the emissive layer from the Al cathode. This is feasible considering the reflected electric field effect from the Al cathode on the device performance, and a suitable electron transport layer (35 nm TPBi) is necessary. A thinner TPBi layer will lead to the quenching of excitons by a reflected electric field from the Al cathode and a thicker one will increase the spontaneous emission rate of the exciton and enhance the efficiency of the device.[28] Consequently, here we can not decrease the TPBi layer to reduce the time of the electron injection into emission layer from the Al cathode and balance the charge injection. As discussed above, increasing the CBP thickness is an alternative and we adopt this strategy in this study. With a thicker CPB spacer, the operation voltage of the device is increased. The turn-on voltages of devices A, B, C, D, and E are 3.0, 2.5, 3.1, 3.5, and 2.6 V, respectively. An increase of 0.9 V (35%) for turn-on voltage is observed in device D. A high turn-on voltage is a

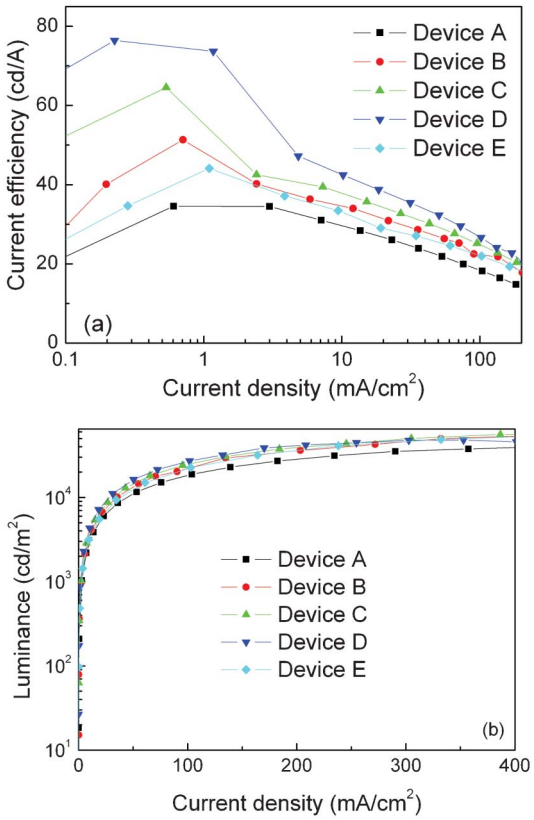

Fig. 3 (a) The current density–efficiency and (b) current density–luminance characteristics of devices A, B, C, D, and E.

disadvantage to OLED applications, so here we have not further increased the CPB thickness and we utilize the 15 nm CBP layer as the optimum thickness. Fig. 3b shows the current density–luminance curves of all the devices. As can be seen, devices B, C, D, and E possess similar luminance under the same current density, while the luminance of device A is very low.

In order explain this phenomenon, we measured the transient resolution photoluminescence (TRPL) of samples S-a, S-b, S-c, S-d, and S-e. The results are shown in Fig. 4a. The lifetimes of $Ir(ppy)_3$ in S-a, S-b, S-c, S-d, and S-e are 447.1, 530.0, 542.2, 536.2, and 534.9 ns, respectively. We can see that the lifetime of the $Ir(ppy)_3$ exciton in S-a is shortened relative to that in S-e (not containing Pt_3Co NPs), which should be due to the exciton quenching by the Pt_3Co NPs. Similar phenomena have also been reported by other groups whereby exciton quenching occurs when the exciton lies near the metal NPs.[29–31] The exciton lifetime in S-b, S-c, S-d, is almost the same as that in S-e due to the introduction of a CBP spacer. It is valuable to note that the lifetimes of all the samples containing Pt_3Co NPs and a spacer are similar, which indicates that the introduction of Pt_3Co NPs has no effect on the spontaneous radiation kinetics of the excitons with a spacer. This result is different from previous reports indicating that the introduction of Au NPs into the device will induce the localized surface plasmon resonance (LSPR)[32,33] and decrease the lifetime of the excitons.[32] In

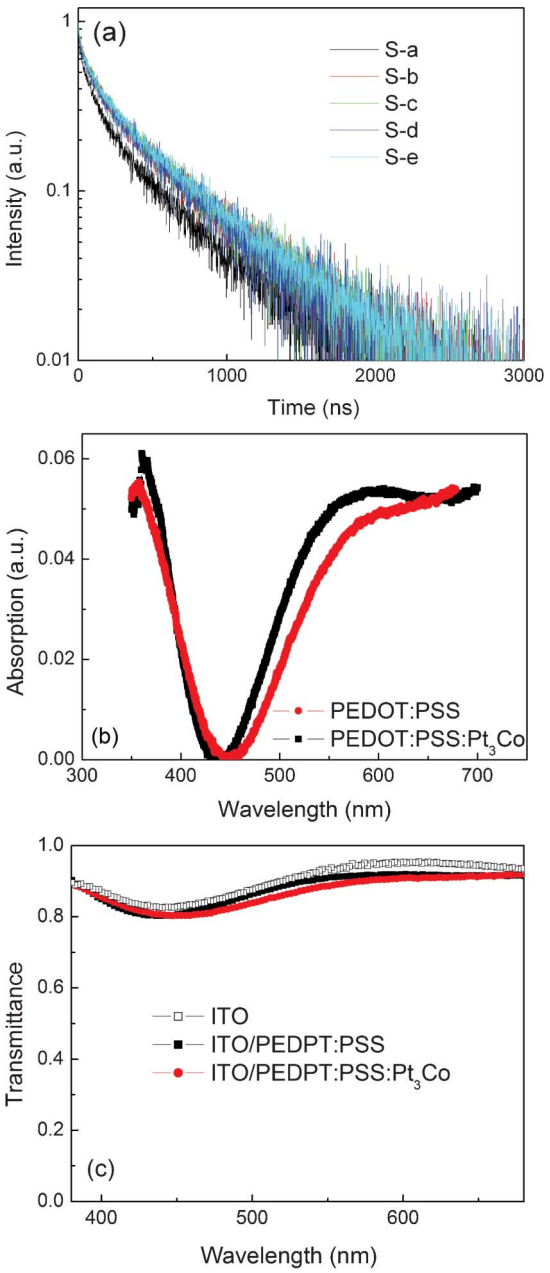

Fig. 4 (a) The time-resolved photoluminescence spectra for samples a–e; (b) the absorption spectra of PEDOT:PSS and PEDOT:PSS:Pt_3Co; (c) the transmittance of ITO, ITO/PEDOT:PSS, and ITO/PEDOT:PSS:Pt_3Co.

addition, the exciton lifetime is smaller than our value reported previously, which is due to the different doping ratio of $Ir(ppy)_3$ in CBP. A higher doping ratio will result in a smaller lifetime due to the concentration quenching by $Ir(ppy)_3$. Fig. 4b shows the absorption spectra of PEDOT:PSS and PEDOT:PSS:Pt_3Co films. We can see that no additional peak is observed on introducing Pt_3Co NPs, which also indicates a lack of or an extremely weak LSPR effect induced by Pt_3Co NPs.

It is necessary to note that the introduction of Pt_3Co NPs into the PEDOT:PSS may change the optical properties of the glass/ITO/HIL structure. Here, we measure the transmittance

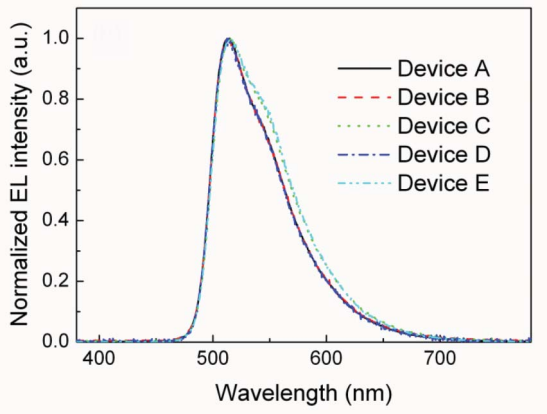

Fig. 5 The normalized EL spectra for devices A, B, C, D, and E.

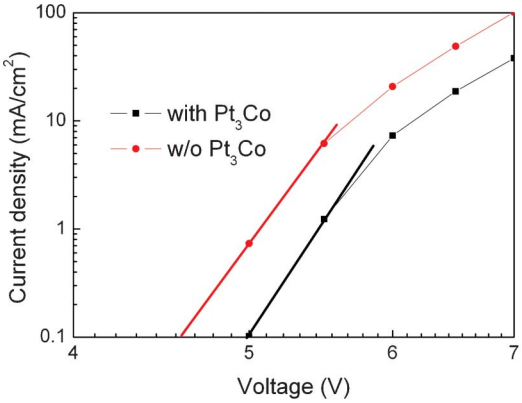

Fig. 7 The voltage–current density characteristics of blue devices with and without Pt_3Co NPs.

of the glass/ITO/HIL structure as well as glass/ITO and the results are shown in Fig. 4c. As can be seen, the transmittance of glass/ITO/PEDOT:PSS is a little lower than that of glass/ITO due to the absorption of PEDOT:PSS, and the introduction of Pt_3Co NPs has a little effect on the transmittance with only a 2% decrease relative to that of glass/ITO/PEDOT:PSS. Fig. 5 shows the normalized electroluminescence (EL) spectra for all the devices. We can see that all the devices possess almost the same EL emission, which indicates that the Pt_3Co NPs have no influence on the exciton decay or the device emission characteristics. In addition, the hole injection and transport characteristics of the devices are further proved by the *J–V* characteristics of the hole-only devices with the structure of ITO/HIL (20 nm)/CBP (80 nm)/Al and the results are shown in Fig. 6. The electron injection from the Al cathode to the CBP is rather limited and can be ignored, this is because the work function of Al is around 4.1 eV, while the lowest unoccupied molecular orbital level (LUMO) of the CBP is around 2.9 eV and there exists a large injection barrier to the electron. The same trend as that of the OLEDs fabricated above is obtained for *J–V* , which further demonstrates that Pt_3Co NPs act as the hole traps due to the negligible electron injection into the devices.

From the discussion above, we can come to the conclusion that the introduction of Pt_3Co NPs only induces the increase of hole-traps in the HIL, consequently balancing the charge injection into the emission layer. The increased hole-trap density due to the Pt_3Co NPs leads to the reduction of hole injections into the device, *i.e.*, a balance charge injection into the emission layer is achieved, which results in a significant enhancement of the EL efficiency, as shown in Fig. 3. Compared with the undoped device (device E), the EL enhancement in device C is estimated to be about 73%.

Furthermore, we also fabricated two blue OLEDs with bis(3,5-difluoro-2-(2-pyridyl)phenyl-(2-carboxypyridyl)) iridium(III) (FIrpic) instead of $Ir(ppy)_3$ with a similar structure to devices D and E, respectively. The doping concentration is 14 vol.% for FIrpic in the CBP host. The current density–voltage characteristics of these two blue devices are shown in Fig. 7, which have the same trend as $Ir(ppy)_3$ based devices where *m* increased upon the introduction of Pt_3Co NPs. Fig. 8 shows the luminance–efficiency characteristics of the blue devices. As can be seen,

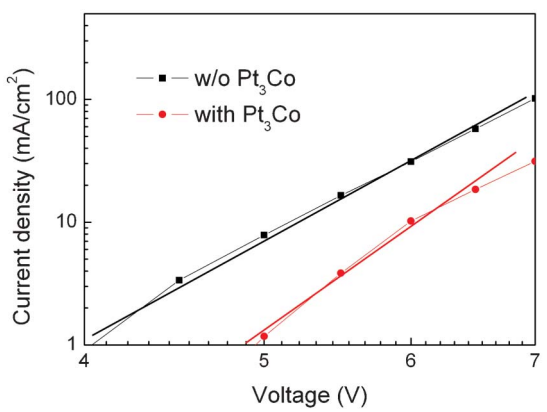

Fig. 6 The current density–voltage characteristics of hole only devices with and without Pt_3Co NPs.

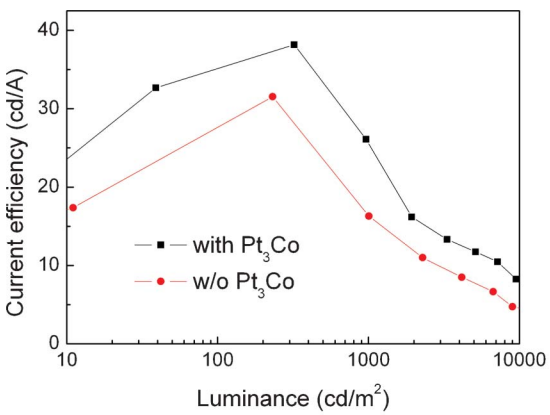

Fig. 8 The luminance–efficiency characteristics of blue devices with and without Pt_3Co NPs.

the current efficiency of the device with Pt_3Co NPs is enhanced by about 32% relative to that without Pt_3Co NPs. These results indicate that a substantial enhancement to the efficiency can be achieved for different color emission OLEDs with the introduction of Pt_3Co.

Conclusions

In conclusion, a highly efficient $Ir(ppy)_3$ based OLED was demonstrated by utilizing a Pt_3Co doped PEDOT:PSS HIL. An enhancement of 73% for peak current efficiency was obtained relative to the device with PEDOT:PSS as the HIL, which is due to a more balanced charge injection in the Pt_3Co containing device. A similar trend was also obtained for FIrpic based blue OLEDs. A conclusion can be drawn that the Pt_3Co introduced in PEDOT:PSS increased the hole traps and suppressed the hole transport in HIL. All of the results provide a new guide for the preparation of efficient OLEDs, *i.e.*, introducing hole traps into HIL or/and HTL to balance the charge injection into the emission layer to improve the performance of OLEDs.

Acknowledgements

This research was supported by the National Natural Science Foundation of China (Nos. 61205025, 61176016, 61275197), Science and Technology Department of Jilin Province (Nos. 20121801, 20110321), the program of CAS Hundred Talents and Key Projects of Science and Technology Development Plan of Jilin Province (Grant No. 20110321).

Notes and references

1 R. H. Jordan, A. Dodabalapur and M. Strukeji, *Appl. Phys. Lett.*, 1996, **68**, 1192.
2 H. Mattoussi, H. Murata, C. D. Merritt, Y. Lizumi, J. Kido and Z. H. Kafafi, *J. Appl. Phys.*, 1999, **86**, 2642.
3 G. Gustafsson, Y. Cao, G. M. Treacy, F. Klavetter, N. Colaneri and A. J. Heeger, *Nature*, 1992, **357**, 477.
4 G. Gu, P. E. Burrows, S. Venkatesh, S. R. Forrest and M. E. Thompson, *Opt. Lett.*, 1997, **22**, 172.
5 J. S. Lewis and M. S. Weaver, *IEEE J. Sel. Top. Quantum Electron.*, 2004, **10**, 45.
6 J. H. Burroughes, D. D. C. Bradley, A. R. Brown, R. N. Marks, K. Mackay, R. H. Friend, P. L. Burns and A. B. Holmes, *Nature*, 1990, **347**, 539–541.
7 P. E. Burrows, G. Gu, V. Bulovic, Z. Shen, S. R. Forrest and M. E. Thompson, *IEEE Trans. Electron Devices*, 1997, **44**, 1188–1203.
8 M. A. Baldo, D. F. O'Brien, M. E. Thompson and S. R. Forrest, *Phys. Rev. B: Condens. Matter Mater. Phys.*, 1999, **60**, 14422–14428.
9 C. Adachi, M. A. Baldo, M. E. Thompson and S. R. Forrest, *J. Appl. Phys.*, 2001, **90**, 5048–5051.
10 V. Bulović, A. Shoustikov, M. A. Baldo, E. Bose, V. G. Kozlov, M. E. Thompson and S. R. Forrest, *Chem. Phys. Lett.*, 1998, **287**, 455–460.
11 S. A. Swanson, G. M. Wallraff, J. P. Chen, W. J. Zhang, L. D. Bozano, K. R. Carter, J. R. Salem, R. Villa and J. C. Scott, *Chem. Mater.*, 2003, **15**, 2305–2312.
12 M. H. Lu and J. C. Sturm, *J. Appl. Phys.*, 2002, **91**, 595–604.
13 C. M. Aguirre, S. Auvray, S. Pigeon, R. Izquierdo, P. Desjardins and R. Martel, *Appl. Phys. Lett.*, 2006, **88**, 183104.
14 L. S. Hung, L. S. Liao, C. S. Lee and S. T. Lee, *J. Appl. Phys.*, 1999, **86**, 4607–4612.
15 Y. Q. Li, L. W. Tan, X. T. Hao, K. S. Ong, F. R. Zhu and L. S. Hung, *Appl. Phys. Lett.*, 2005, **86**, 153508.
16 S. Yu, D. Huang, Y. Chen, K. Wu and Y. i. Tao, *Langmuir*, 2012, **28**, 424–430.
17 C. I. Wu, C. T. Lin and Y. H. Chen, *Appl. Phys. Lett.*, 2006, **88**, 152104.
18 Y. Cai, H. X. Wei, J. Li, Q. Y. Bao, X. Zhao, S. T. Lee, Y. Q. Li and J. X. Tang, *Appl. Phys. Lett.*, 2011, **98**, 113304.
19 J.-H. Lee, D.-S. Leem, H.-J. Kim and J.-J. Kim, *Appl. Phys. Lett.*, 2009, **94**, 123306.
20 M. Kröger, S. Hamwi, J. Meyer, T. Riedl, W. Kowalsky and A. Kahn, *Org. Electron.*, 2009, **10**, 932–938.
21 J. Meyer, S. Hamwi, M. Kröger, W. Kowalsky, T. Riedl and A. Kahn, *Adv. Mater.*, 2012, **24**, 5408–5427.
22 S. Y. Kim, W. S. Jeon, T. J. Park, R. Pode, J. Jang and J. H. Kwon, *Appl. Phys. Lett.*, 2009, **94**, 133303.
23 A. J. Campbell, D. D. C. Bradley and D. G. Lidzey, *J. Appl. Phys.*, 1997, **82**, 6326–6342.
24 C. Wang, D. van der Vliet, K. C. Chang, H. You, D. Strmcnik, J. A. Schlueter, N. M. Markovic and V. R. Stamenkovic, *J. Phys. Chem. C*, 2009, **113**, 19365–19368.
25 C.-J. Sun, Y. Wu, Z. Xu, B. Hu, J. Bai, J. P. Wang and J. Shen, *Appl. Phys. Lett.*, 2007, **90**, 232110.
26 B. Hu, Y. Wu, Z. Zhang, S. Dai and J. Shen, *Appl. Phys. Lett.*, 2006, **88**, 022114.
27 C. Wang, D. van der Vliet, K.-C. Chang, H. You, D. Strmcnik, J. A. Schlueter, N. M. Markovic and V. R. Stamenkovic, *J. Phys. Chem. C*, 2009, **113**, 19365–19368.
28 D. D. Song, S. L. Zhao and H. Aziz, *Adv. Funct. Mater.*, 2011, **21**, 2311–2317.
29 S. Mayilo, M. A. Kloster, M. Wunderlich, A. Lutich, T. A. Klar, A. Nichtl, K. Kürzinger, F. D. Stefani and J. Feldmann, *Nano Lett.*, 2009, **9**, 4558–4563.
30 G. Schneider, G. Decher, N. Nerambourg, R. Praho, M. H. V. Werts and M. Blanchard-Desce, *Nano Lett.*, 2006, **6**, 530–536.
31 J. R. Lakowicz, K. Ray, M. Chowdhury, H. Szmacinski, Y. Fu, J. Zhang and K. Nowaczyk, *Analyst*, 2008, **133**, 1308–1346.
32 W. Y. Ji, L. T. Zhang and W. F. Xie, *Opt. Lett.*, 2012, **37**, 2019–2021.
33 Y. Su, Y. Ke, S. Cai and Q. Yao, *Light: Sci. Appl.*, 2012, **1**, e14.